Composites Part C: Open Access 19 (2026) 100701

Contents lists available at ScienceDirect

Composites Part C: Open Access

journal homepage: www.elsevier.com/locate/composites-part-c-open-access

# Why selected autoclave-cured Double–Double laminates are particular prone to warpage

Erik Kappel [a,*], Ronald Klomp [b]

[a] DLR, Institute of Lightweight Systems (SY), Lilienthalplatz 7, 38108 Braunschweig, Germany
[b] Royal NLR - Netherlands Aerospace Centre, Voorsterweg 31, 8316 PR Marknesse, The Netherlands

ARTICLE INFO

*Keywords:*
Composite design
Double–double
Process-induced distortions
Warpage

ABSTRACT

Double–Double (DD) laminates provide unique design and manufacturing opportunities. This makes them a promising challenger for conventional laminates used in aerospace composite parts today. DD laminates benefit from an effect denoted as 'homogenization', which leads to a mechanical behavior known from orthotropic laminates, without complex coupling effects, although DD laminates have asymmetric ply-stacking sequences. Manufacturing aspects and particularly the topic of process-induced distortions (PID) have attracted little attention in DD context. The present article is dedicated to this topic. It outlines why some DD laminates show warpage and twist after a typical 180°C curing process, while others remain almost flat. Hence, the article provides practical guidance for selecting building-block stacking sequences, which induce minimum warpage.

## 1. Motivation

Dimensional fidelity is an important requirement for aerospace composites. This is true for parts made with conventional laminates, but also for parts made from Double–Double laminates. The later belongs to the group of so-called unconventional laminates (UCL). While design [1–3] and optimization aspects [4–8] for DD laminates have been addressed in dedicated studies, the manufacturing-related topic of process-induced distortions (PID) has attracted little attention up to now. The following section provides and overview of sources for unwanted part deformations and limits the relevant drivers in focus of the present paper.

### 1.1. Reasons for warpage and twist of carbon-fiber-thermoset laminates, autoclave cured at elevated temperatures

Unwanted, non-trivial part deformations accompany composite manufacturing inevitably [9]. Fernlund and Poursartip summarize it excellently with: 'Composite parts will never have the same dimensions as the tool they were made on' [10]. The origins are manifold and could not all be discussed in detail here, without diluting the article's focus. However, the following list shall briefly outline well examined drivers for unwanted part distortions in composite manufacturing context.

- *Reversible & irreversible effects*: Curing a typical aerospace-grade, carbon-fiber epoxy prepreg, in a high-temperature (e.g. 180°C) autoclave process, results in reversible and irreversible effects. The thermoset matrix curing is irreversible. Curing-induced volumetric shrinkage of the neat resin distributes to the plies principal directions, which leads to contraction. The temperature drop, during the cool down from curing to room temperature, induces thermo-elastic contraction of the matrix, with its comparably high CTE. The related strains lead to shape changes.
- *Globally orthotropic material properties*: Unidirectional(UD)-ply-based composite laminates have fiber-dominated in-plane properties and resin dominated out-of-plane properties. As through-thickness strains due to chemical shrinkage or thermal expansion in in-plane $\varepsilon_z^{T,C} \gg (\varepsilon_x^{T,C}, \varepsilon_y^{T,C})$ [9,11,12]. This inevitable leads to the fact that a curved composite sections deform, which is well known as the driver for Spring-in (see for example [13]) distortions.
- *Residual stresses*: A composite laminate is a stack of numerous individual differently oriented unidirectional (UD) plies. Each ply shows for example the same thermal expansion behavior with respect to their local coordinate system, with $\alpha_1 \ll \alpha_2$. However, due to the plies' different orientation in the global laminate coordinate system the individual expansion/contraction characteristic is constrained. Residual stress inevitably build up. As long a laminate stacks are symmetric, those stresses balance out, and no warpage of a flat part is observed. Asymmetric laminate usually deform after a high-temperature manufacturing process.

* Corresponding author.
*E-mail address:* erik.kappel@dlr.de (E. Kappel).

https://doi.org/10.1016/j.jcomc.2026.100701
Received 7 August 2025; Received in revised form 14 January 2026; Accepted 21 January 2026
Available online 22 January 2026

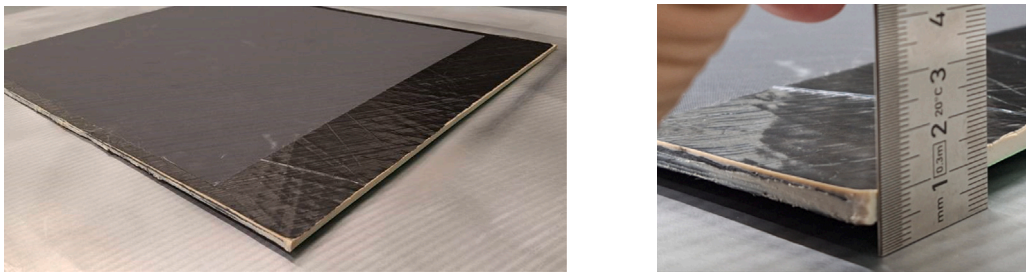

(a) (b)

**Fig. 1.** Warpage of a 400 mm × 500 mm CFRP Double–Double laminate. Courtesy: NLR.

- *Tool-part interaction*: Warpage of thin laminates ≈(< 1.0 mm) can arise from a CTE mismatch between the manufacturing tool and the composite laminate cured on it. In particular, single-sided tool concepts are prone to produced warpage, as the stresses due to the CTE-mismatch are introduced in the laminate only at the tool-part interface. This, leads to pre-stressing of plies close to the tool. Once, the part is fully cured and cooled down, those introduced stresses redistribute, which usually results in considerable warpage of samples. [12,14]
- *Forced-interaction*: Forced-interaction is related to the scenario, when a composite laminate is partially wrapped around a male tool, with a CTE higher than the composite CTE. Acting autoclave pressure enforces the laminate to stay in contact with the expanding tool during the process. Interaction between the part and the tool induces an asymmetric residual stress state, similar as for the tool-part interaction effect. However, it has been shown that forced interaction can lead to deformation of even thick laminates with symmetric stackings [15].
- *Fiber-volume fraction gradients*: Coefficients of thermal expansion of a single ply depend on the ply's fiber and resin content $\alpha_1, \alpha_2 = f(V_f)$, as can be seen when typical rules of mixture are examined. Selected manufacturing and bagging scenarios can lead to resin squeeze/bleed, as for example a single peel ply on top of a laminate, in a single-sided manufacturing scenario. Resin is soaked by the peel ply during the process, which can lead to fiber-volume fraction gradients in the laminates thickness direction. This affects the local laminate properties. Once the peel-ply is removed, initially flat parts deform. Thermo-elastic warpage can be the consequence, even though the laminate stacking sequence is symmetric.

The present article focuses on the most simple geometrical case. Laminates in focus are cured on a flat tool. A double-sided tool approach is used for the samples, with a no-bleed vacuum bagging setup being applied. Thus, the extrinsic effects forced-interaction and tool-part interaction are considered irrelevant for the parts at hand. $V_f$-gradients are also considered as irrelevant, due to the use of a double-sided tool and no use of peel plies on the laminate surfaces.

In context of compression-after-impact (CAI) sample manufacturing, Double–Double panels were manufactured by the authors. Remarkable warpage was observed, which was surprising at first sight. Fig. 1 shows the manufactured 400 mm × 500 mm, 20-ply panel after demolding.

The approximately 4.2 mm thick panels showed considerable warpage of multiple mm. This was unexpected, as the selected four-ply Building Block (BB) stacking sequence $[15, -55, -15, 55]$ was chosen carefully, to promote 'homogenization' of the DD laminate. In addition, five BB repeats ($r = 5$) were realized for the 20-ply laminate. The present article aims to explain the unexpected high deformations.

It this context it is highlighted that Hawkins et al. [16] published a comprehensive study on warpage of Double–Double laminates, parallel to the composition of the present manuscript. Aside from baseline DD laminates, the authors presented also new particular stacking sequences. Those are termed symmetry-enhanced-Double–Double (SEDD), being introduced as SEDD-1 : $[(BB)_s/(BB)_r]_T$ and SEDD-2 with $[(BB)_{s,r}/(BB)_n]_T$, wherein $s, r$ indicating symmetry and the number of BB-repeats, respectively. $_T$ denotes 'total' as outlined in [17].

**Table 1**
All 24 conceivable BB stacking sequences.

| BB layup | BB layup | BB layup | BB layup |
|---|---|---|---|
| [15, −15, 55, −55] | [−15, 15, 55, −55] | [55, 15, −15, −55] | [−55, 15, −15, 55] |
| [15, −15, −55, 55] | [−15, 15, −55, 55] | [55, 15, −55, −15] | [−55, 15, 55, −15] |
| [15, 55, −15, −55] | [−15, 55, 15, −55] | [55, −15, 15, −55] | [−55, −15, 15, 55] |
| [15, 55, −55, −15] | [−15, 55, −55, 15] | [55, −15, −55, 15] | [−55, −15, 55, 15] |
| [15, −55, −15, 55] | [−15, −55, 15, 55] | [55, −55, 15, −15] | [−55, 55, 15, −15] |
| [15, −55, 55, −15] | [−15, −55, 55, 15] | [55, −55, −15, 15] | [−55, 55, −15, 15] |

Hawkins et al.' results for baseline DD laminates are particular relevant for the study at hand, as they substantiate the findings later presented in this article. The authors present a conventional DD laminate with the stacking $[+9/-61.5/+61.5/-9]_5$, which showed minimum warpage. As will be seen later the particular BB characteristic $[\pm\varphi, \mp\psi, \pm\psi, \mp\varphi]$ is also identified as the minimum-warpage sequence in the present article.

### 1.2. A brief intro to DD

Double–Double laminates belong to the UCL group. An overview of recent activities in DD context can be found in [6]. In its initial laminate description [1] a DD laminate is described by the notation $[\pm\varphi, \pm\psi]_r$. In context of dry-fiber materials, $\pm\varphi$ refers to one layer of a crimped biaxial material. In unidirectional (UD) prepreg context, a Building Block is usually described by a 4-ply sequence, such as $[\varphi, -\psi, -\varphi, \psi]_r$, for example. 24 conceivable BB stackings exist.

Table 1 shows them, while in conjunction with the aforementioned OHT and CAI activities, the ply orientations $|\varphi| = 15$, $|\psi| = 55$ are considered hereafter only, for sake of conciseness.

A DD laminate consists of a sequence of BBs. A requirement for symmetry does not exist. A DD laminate is asymmetric, but always balanced, due to the BB architecture. The parameter $r$ quantifies the number of BB repeats. The laminate thickness is determined by $t_{lam} = 4 \cdot r \cdot t_{ply}$. The typical notation is deduced from the classical-laminate theory (CLT) [17], as presented hereafter.

$$\underbrace{\begin{bmatrix} N \\ M \end{bmatrix} = \begin{bmatrix} A & B \\ B & D \end{bmatrix} \cdot \begin{bmatrix} \varepsilon_0 \\ \varkappa \end{bmatrix}}_{\text{CLT}} \quad , \quad \underbrace{\begin{bmatrix} \sigma \\ \sigma^f \end{bmatrix} = \begin{bmatrix} A^* & B^* \\ 3B^* & D^* \end{bmatrix} \cdot \begin{bmatrix} \varepsilon_0 \\ \varepsilon^f \end{bmatrix}}_{\text{typical DD notation}} \tag{1}$$

with the 'thickness-normalized' matrices $[A^*] = [A]/t_{lam}$, $[B^*] = 2[B]/t_{lam}^2$ and $[D^*] = 12 \cdot [D]/t_{lam}^3$ (A more detailed derivation is provided in [8]). The process of 'homogenization' is often cited in DD context. It describes how the laminate-asymmetry induced coupling coefficients, in the [ABD] matrix, and/or its thickness-term-normalized equivalent [A*B*D*], diminish with increasing BB repeats $r$. Basically

**Table 2**
M21E/IMA prepreg parameters. ppm denotes parts-per-million ($10^{-6}$).

| Property | $E_1$ | $E_2$ | $\nu_{12}$ | $G_{12}$ | $\alpha_1$ | $\alpha_2$ | $t_{ply,nominal}$ |
|---|---|---|---|---|---|---|---|
| Unit | GPa | GPa | – | GPa | ppm/K | ppm/K | mm |
| Value | 154.0 | 8.5 | 0.32 | 4.2 | 1.5 | 32.2 | 0.184 |
| Source | [18] | [18] | [18] | [18] | [19] | [19] | – |

one finds that all coefficients of the $[B^*]$ matrix scale with $1/r$. The bending–twist coupling coefficients, $D^*_{16}$ and $D^*_{26}$, scale proportional with $1/r^2$.

$$[B^*] \propto \frac{1}{r} \quad \text{and} \quad [D^*] = \begin{bmatrix} \cancel{f(r)} & \cancel{f(r)} & \frac{1}{r^2}\cdot(\ldots) \\ \cancel{f(r)} & \cancel{f(r)} & \frac{1}{r^2}\cdot(\ldots) \\ \frac{1}{r^2}\cdot(\ldots) & \frac{1}{r^2}\cdot(\ldots) & \cancel{f(r)} \end{bmatrix} . \tag{2}$$

This 'homogenization' basically leads to a simplified mechanical behavior of a laminate. It uncouples in-plane tension and shear, bending and twisting, as well as the global coupling of the aforementioned in-plane and out-of-plane effects, as it is indicated hereafter by the population of the [A*B*D*] matrix.

$$\begin{bmatrix} A^* & B^* \\ 3B^* & D^* \end{bmatrix} = \begin{bmatrix} \bullet & \bullet & 0 & \approx 0 & \approx 0 & \approx 0 \\ \bullet & \bullet & 0 & \approx 0 & \approx 0 & \approx 0 \\ 0 & 0 & \bullet & \approx 0 & \approx 0 & \approx 0 \\ \approx 0 & \approx 0 & \approx 0 & \bullet & \bullet & \approx 0 \\ \approx 0 & \approx 0 & \approx 0 & \bullet & \bullet & \approx 0 \\ \approx 0 & \approx 0 & \approx 0 & \approx 0 & \approx 0 & \bullet \end{bmatrix} \quad \text{for } r \gg 1 \quad . \tag{3}$$

The population equals the one of both homogeneous isotropic and orthotropic materials, which explains the phrase 'homogenization'. Most studies in DD context focus on those briefly outlined dependencies in context with the $[ABD]$ matrix. The effect of manufacturing and in particular high-temperature curing remains widely disregarded and in particular the relevant drivers for warpage $N^T$ and $M^T$ are not examined. Earlier studies, on a tapered omega-shaped stiffener (Chapter 3 in [2]), showed that the actual building-block stacking sequence affects part deformation, but the effect was neither generalized to other DD laminates nor assessed for all conceivable BB stackings.

## 2. Numerical cool-down analyses

FE-model based cool-down analysis are a practical approach to assess and visualize, laminate-asymmetry-induced warpage of composite structures. Therefore, this type of analysis is used hereafter to interrelate the BB stacking sequences and corresponding part deformations due to manufacturing. Hexcel's M21E/IMA prepreg is considered in the following FE analyses. The corresponding ply data is summarized in Table 2.

However, it shall be highlighted, that the recommendations, deduced hereafter, are also valid for other UD prepreg materials, as long those can be considered as 'similar' in terms of stiffness ratio, CTE ratio and curing temperature.

### 2.1. FE model description

The examined FE models were created in ABAQUS CAE 6.14. A quadratic plate, with 500 mm × 500 mm, is modeled, using the ABAQUS' composite modeler. The simulation mimics a cool-down from the curing temperature of 180°C to 20°C room temperature, which is equivalent to the modeled temperature change of $\Delta T = -160$ K (Note that a parametric ABAQUS input-file is provided in the Appendix). Table 3 provides an example result (case $[55, -55, 15, -15]$ from Table 1) and outlines additional modeling settings. All BB-case comparisons hereafter refer to out-of-plane displacements ($z$-direction, $U_3$ in ABAQUS) of the modeled flat part, whose edges illustrated as black lines in all plots in undeformed state are.

Model execution as well as output plotting were executed script based. Thus, all plots hereafter are directly comparable, as legend thresholds, view settings as well as the magnification setting (= 1) are identical in all plots.

### 2.2. Numerical study - result overview

The described numerical analysis have been executed for all 24 BB cases, while four BB-repeats ($r = 4$) are considered. Thus, the examined 16-ply laminates are 2.944 mm thick. Fig. 2 summarizes all results. Note, that the corresponding BB stackings are provided in each picture, for the readers' convenience.

At first sight, the plots allow for the following observations:

1. Only two cases apparently show almost no/little warpage/ deformation.
2. One can further distinguish in cases showing either upward or downward displacements
3. Twist is observed, almost in all cases.

A more detailed comparison of the individual results reveals, that for stackings belonging to the $[\pm\varphi, \mp\psi, \pm\psi, \mp\varphi]$ group, mirroring the stacking sequence results in a mirrored out-of-plane displacement characteristic. The effect can be seen well for the pair $[15, 55, -55, -15]$/ $[-15, -55, 55, 15]$, for example. Later the presented analyses show that mirroring a BB stacking results in a sign change of the curvature vector coefficient $\varkappa^T_{xy}$, which explains the observed 'mirror'-effect on the deformation characteristic.

## 3. A study on the origins for warpage

In fact, DD's asymmetric laminate stacking results in thermal-contraction induced in-plane forces and out-of-plane moments. Those are defined as

$$\begin{bmatrix} N^T_x \\ N^T_y \\ N^T_{xy} \end{bmatrix} = \sum_{k=1}^{n} [\bar{Q}]_k \begin{bmatrix} \varepsilon^T_x \\ \varepsilon^T_y \\ \gamma^T_{xy} \end{bmatrix}_k \cdot t_{ply} \quad , \quad \begin{bmatrix} M^T_x \\ M^T_y \\ M^T_{xy} \end{bmatrix} = \sum_{k=1}^{n} [\bar{Q}]_k \begin{bmatrix} \varepsilon^T_x \\ \varepsilon^T_y \\ \gamma^T_{xy} \end{bmatrix}_k \cdot \frac{1}{2}\cdot\left(h_k^2 - h_{k-1}^2\right) . \tag{4}$$

For symmetric laminates, one observes $\begin{bmatrix} M^T_x & M^T_y & M^T_{xy} \end{bmatrix}^T = \vec{0}$. In addition, $[B]$ equals zero, which explains that a symmetric laminate only shows in-plane contraction/ expansion, but remains flat after the cool-down from the curing temperature, although $[D]^{-1} \neq [0]$.

$$\begin{bmatrix} \varepsilon^0_x \\ \varepsilon^0_y \\ \gamma^0_{xy} \\ \varkappa_x \\ \varkappa_y \\ \varkappa_{xy} \end{bmatrix} = \begin{bmatrix} [A] & [B] \\ [B] & [D] \end{bmatrix}^{-1} \cdot \begin{bmatrix} N^T_x \\ N^T_y \\ N^T_{xy} \\ M^T_x \\ M^T_y \\ M^T_{xy} \end{bmatrix} = \begin{bmatrix} [a] & [b] \\ [b] & [d] \end{bmatrix} \cdot \begin{bmatrix} N^T_x \\ N^T_y \\ N^T_{xy} \\ M^T_x \\ M^T_y \\ M^T_{xy} \end{bmatrix} \tag{5}$$

For DD laminates it is essential to consider both $\vec{N}^T$ and $\vec{M}^T$ vectors, as well as the $[a]$, $[b]$ and $[d]$ matrices. Both vectors will always be $\neq \vec{0}$ for DD. Thus, they contribute to in-plane strains and out-of-plane warpage and twist, which can be seen above in Fig. 2. The following expression shows the different contributions for symmetric and asymmetric laminates.

$$\begin{bmatrix} \varepsilon^0_x & \varepsilon^0_y & \gamma^0_{xy} \end{bmatrix}^T = \underbrace{[a] \cdot \begin{bmatrix} N^T_x & N^T_y & N^T_{xy} \end{bmatrix}^T}_{\neq\vec{0},\ (\neq\vec{0} \text{ for symmetric laminate})} + \underbrace{[b] \cdot \begin{bmatrix} M^T_x & M^T_y & M^T_{xy} \end{bmatrix}^T}_{\neq\vec{0},\ (=\vec{0} \text{ for symmetric laminate})}$$

**Table 3**
Example result (case [55, −55, 15, −15] from Table 1) and additional FE model parameters.

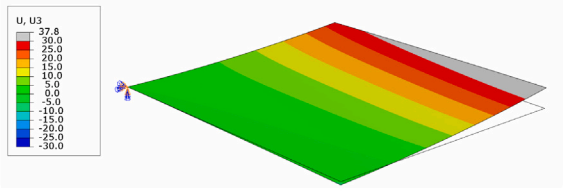


- 2500 4-node S4R elements (50 × 50, 10 mm edge length)
- out-of-plane displacement $U_3$ in range −30/+30 mm
- Boundaries: $U1 = U2 = U3 = UR1 = UR2 = UR3$ at node 1
- Geometrically nonlinear calculation, 'nlgeom = YES'

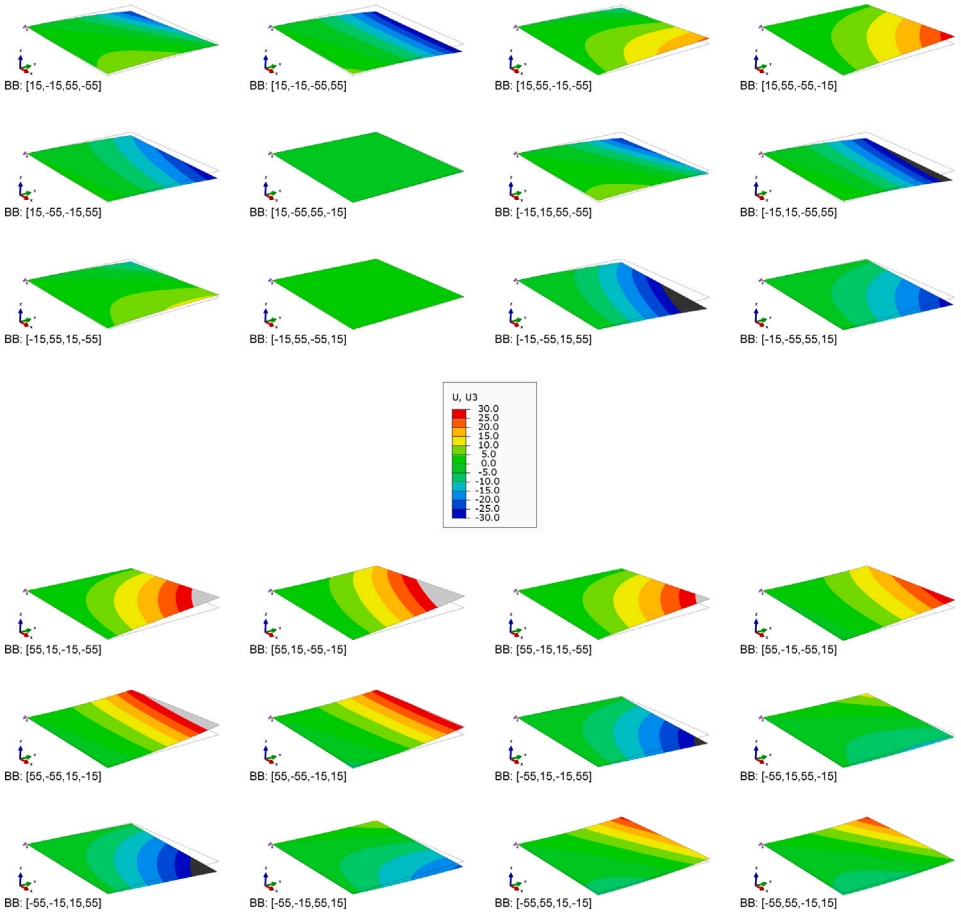


**Fig. 2.** Distortion plots of all 24 conceivable building-block configuration $[\pm 15°/\pm 55°]_4$, for $t_{ply} = 0.184$ mm. The reader is referred to the PDF version of the article for improved readability.

$$\begin{bmatrix} \varkappa_x & \varkappa_y & \varkappa_{xy} \end{bmatrix}^T = \underbrace{[b] \cdot \begin{bmatrix} N_x^T & N_y^T & N_{xy}^T \end{bmatrix}^T}_{\neq \vec{0},\ (=\vec{0} \text{ for symmetric laminate})} + \underbrace{[d] \cdot \begin{bmatrix} M_x^T & M_y^T & M_{xy}^T \end{bmatrix}^T}_{\neq \vec{0},\ (=\vec{0} \text{ for symmetric laminate})} \tag{6}$$

The extension-bending stiffness matrix plays a key role. It is defined as

$$[B] = \frac{1}{2} \cdot \sum_{k=1}^{n} [\bar{Q}]_k \cdot \left(h_k^2 - h_{k-1}^2\right) \quad . \tag{7}$$

It is well known from conventional laminates, that laminate symmetry leads to $[B] = [0]$, driven by the $\left(h_k^2 - h_{k-1}^2\right)$ term, which induces a sign change for a ply positioned symmetrically above or below the laminates' mid plane. This behavior transfers similarly to the thermal moment vector $\vec{M}^T = \begin{bmatrix} M_x^T & M_y^T & M_{xy}^T \end{bmatrix}^T$. For symmetric laminates $\vec{M}^T = \vec{0}$. Thus, a flat laminate will not bend when subjected to a temperature change. It will only show in-plane elongation, which refers to the laminates' CTEs $\alpha_x, \alpha_y$ and $\alpha_{xy}$. Double–Double laminates are asymmetric. Thus, $\vec{M}^T \neq \vec{0}$ must be considered.

As the ABD matrix population state from Eq. (3) is not perfectly reached, the curvatures depend on contributions from $[b] \cdot \vec{N}^T$ and $[d] \cdot \vec{M}^T$. Analyzing the relations above from a DD perspective allow for some cognition.

The notation

$$BB := [bb_1, bb_2, bb_3, bb_4] \tag{8}$$

is introduced for the four-ply building block angle, for the subsequent analysis. For a DD laminate, made from plies with a constant ply thickness $t_{ply}$, the force vector can be written as follows,

$$\begin{bmatrix} N_x^T \\ N_y^T \\ N_{xy}^T \end{bmatrix} = \sum_{k=1}^{n} [\bar{Q}]_k \begin{bmatrix} \varepsilon_x^T \\ \varepsilon_y^T \\ \gamma_{xy}^T \end{bmatrix}_k \cdot t_{ply} = t_{ply} \cdot \sum_{k=1}^{n} [T]_k^{-1} \cdot [Q] \cdot \begin{bmatrix} \alpha_1 \\ \alpha_2 \\ 0 \end{bmatrix} \cdot \Delta T$$

$$= r \cdot t_{ply} \cdot \underbrace{\left([T]_{bb_1}^{-1} + [T]_{bb_2}^{-1} + [T]_{bb_3}^{-1} + [T]_{bb_4}^{-1}\right)}_{\begin{bmatrix} \bullet & \bullet & 0 \\ \bullet & \bullet & 0 \\ 0 & 0 & \bullet \end{bmatrix}} \cdot \underbrace{[Q] \cdot \begin{bmatrix} \alpha_1 \\ \alpha_2 \\ 0 \end{bmatrix}}_{\begin{bmatrix} \bullet \\ \bullet \\ 0 \end{bmatrix}} \cdot \Delta T$$

with $[T]_k^{-1}$ being defined according to Eq. (13). This leads to the generalization of the in-plane force vector for all conceivable DD laminates.

$$N_x^T, N_y^T \neq 0 \text{ and } N_{xy}^T = 0 \tag{9}$$

The moment vector can be written as

$$\begin{bmatrix} M_x^T \\ M_y^T \\ M_{xy}^T \end{bmatrix} = \sum_{k=1}^{n} [\bar{Q}]_k \begin{bmatrix} \varepsilon_x^T \\ \varepsilon_y^T \\ \gamma_{xy}^T \end{bmatrix}_k \cdot \frac{t_{ply}}{2} \cdot (h_k + h_{k-1}) \quad .$$

Introducing the DD-specific relations

$$h_k = -4 \cdot r \cdot t_{ply}/2 + k \cdot t_{tply}, \quad h_{k-1} = -4 \cdot r \cdot t_{ply}/2 + (k-1) \cdot t_{tply} \tag{10}$$

allows for the reformulation to

$$\begin{bmatrix} M_x^T \\ M_y^T \\ M_{xy}^T \end{bmatrix} = \sum_{k=1}^{n} [\bar{Q}]_k \begin{bmatrix} \varepsilon_x^T \\ \varepsilon_y^T \\ \gamma_{xy}^T \end{bmatrix}_k \cdot \frac{t_{ply}^2}{2} (-4r + 2k - 1) \quad .$$

With inserting

$$[\bar{Q}] = [T]^{-1}[Q][T]^{-T} \quad \text{and} \quad \begin{bmatrix} \varepsilon_x^T \\ \varepsilon_y^T \\ \gamma_{xy}^T \end{bmatrix} = [T]^T \cdot \begin{bmatrix} \alpha_1 \\ \alpha_2 \\ 0 \end{bmatrix} \cdot \Delta T \tag{11}$$

one finds

$$\begin{bmatrix} M_x^T \\ M_y^T \\ M_{xy}^T \end{bmatrix} = \frac{t_{ply}^2}{2} \left( \sum_{k=1}^{n} [T]_k^{-1} \cdot (-4r + 2k - 1) \right) \cdot [Q] \cdot \begin{bmatrix} \alpha_1 \\ \alpha_2 \\ 0 \end{bmatrix} \cdot \Delta T \tag{12}$$

It is important to highlight the effect of the ply-angle sign on the inverted transformation matrix for the following analyses. It is hereafter outlined for ply angles $\varphi$ and $-\varphi$.

$$[T]^{-1}(\phi) = \begin{bmatrix} c^2 & s^2 & -2sc \\ s^2 & c^2 & 2sc \\ sc & -sc & c^2 - s^2 \end{bmatrix} \quad , \quad [T]^{-1}(-\phi) \begin{bmatrix} c^2 & s^2 & 2sc \\ s^2 & c^2 & -2sc \\ -sc & sc & c^2 - s^2 \end{bmatrix} \quad , \tag{13}$$

with $c, s$ denoting cosine and sine, respectively.

The ply-angle sign effect affects the term

$$\left( \sum_{k=1}^{n=4r} [T]_k^{-1} \cdot (-4r + 2k - 1) \right) \tag{14}$$

in Eq. (12), which requires particular attention. The following example shows how the individual contribution of a single ply in the BB can be quantified. With $r = 2$ (eight-ply laminate) one finds

$$\begin{aligned} (\,) &= \left( -7[T]_{bb_1}^{-1} - 5[T]_{bb_2}^{-1} - 3[T]_{bb_3}^{-1} - [T]_{bb_4}^{-1} + [T]_{bb_1}^{-1} + 3[T]_{bb_2}^{-1} \right. \\ &\quad \left. + 5[T]_{bb_3}^{-1} + 7[T]_{bb_4}^{-1} \right) \\ &= \left( -6[T]_{bb_1}^{-1} - 2[T]_{bb_2}^{-1} + 2[T]_{bb_3}^{-1} + 6[T]_{bb_4}^{-1} \right) \end{aligned}$$

This term can be transferred to

$$\left[ [T]_{bb_1}^{-1}, [T]_{bb_2}^{-1}, [T]_{bb_3}^{-1}, [T]_{bb_4}^{-1} \right] \cdot \left[ c(bb_1), c(bb_2), c(bb_3), c(bb_4) \right]^T \quad , \tag{15}$$

with $c(bb_i)$ referring to the summed contribution of the ply $bb_i$ in the BB. This step basis on the repetitive pattern of a DD laminate. The value $c(bb_1)$, for example, denotes the contribution of all $bb_1$ plies in the laminate. For a 20-ply laminate ($r = 5$), $c(bb_1)$ equals the sum of five individual contributions of ply $bb_1$. The reformulation allows for quantifying the contribution of the specific building-block plies depending on the number of repeats. Table 4 provides the individual ply contribution for multiple repeat cases.

**Table 4**
BB ply contribution for different number of repeats.

| Case | $c(bb_1)$ | $c(bb_2)$ | $c(bb_3)$ | $c(bb_4)$ |
|---|---|---|---|---|
| $r = 1$ | −3 | −1 | 1 | 3 |
| $r = 2$ | −6 | −2 | 2 | 6 |
| $r = 3$ | −9 | −3 | 3 | 9 |
| $r = 4$ | ... | ... | ... | ... |

The previous table shows that the ply contributions can be generalized as follows

$$\left[ [T]_{bb_1}^{-1}, [T]_{bb_2}^{-1}, [T]_{bb_3}^{-1}, [T]_{bb_4}^{-1} \right] \cdot [-3, -1, 1, 3]^T \cdot r \quad . \tag{16}$$

Introducing in Eq. (12) yields the DD specific formulation for the moment-vector:

$$\begin{bmatrix} M_x^T \\ M_y^T \\ M_{xy}^T \end{bmatrix} = \frac{t_{ply}^2}{2} \cdot \left( -3[T]_{bb_1}^{-1} - [T]_{bb_2}^{-1} + [T]_{bb_3}^{-1} + 3[T]_{bb_4}^{-1} \right) \cdot r \cdot [Q] \cdot \begin{bmatrix} \alpha_1 \\ \alpha_2 \\ 0 \end{bmatrix} \cdot \Delta T \quad . \tag{17}$$

Due to the individual scalar pre-factors of the BB-ply specific transformation matrices, only one particular case is found. Only with $|bb_1| = |bb_4|$ and $|bb_2| = |bb_3|$, specific contributions blank-out each other. For those cases, one will always see a matrix population of type

$$\left( -3[T]_{bb_1}^{-1} - [T]_{bb_2}^{-1} + [T]_{bb_3}^{-1} + 3[T]_{bb_4}^{-1} \right) \quad \rightarrow \quad \begin{bmatrix} 0 & 0 & \bullet \\ 0 & 0 & \bullet \\ \bullet & \bullet & 0 \end{bmatrix} \quad . \tag{18}$$

When this population is combined with

$$[Q] \cdot \begin{bmatrix} \alpha_1 \\ \alpha_2 \\ 0 \end{bmatrix} \cdot \Delta T \quad \rightarrow \quad \begin{bmatrix} \bullet \\ \bullet \\ 0 \end{bmatrix} \quad , \tag{19}$$

one will always find $M_x^T = M_y^T = 0$ ('no bending') and $M_{xy}^T \neq 0$ ('non-zero twist').

Thus, the analysis reveals only two particular cases .

$$N^T = [\neq 0, \neq 0, 0]^T \text{ and}$$

$$M^T = \begin{cases} [0, 0, \neq 0]^T & , \text{ when } |bb_1| = |bb_4| \text{ and } |bb_2| = |bb_3| \\ [\neq 0, \neq 0, \neq 0]^T & , \text{ all remaining} \end{cases} \tag{20}$$

for all DD laminates.

### 3.1. Intermediate summary

The previous analyses show that all 24 conceivable BB stackings can be divided into only two distinct groups. Their corresponding matrix populations are outlined in Table 5.

The 'twist-only' group contains 8 out of 24 cases and is characterized by the BB pattern $|bb_1| = |bb_4|$ and $|bb_2| = |bb_3|$. Cooling down a laminate of this group leads to shear-free in-plane distortions ($\gamma_{xy}^T = 0$), superposed by a twist-only out-of-plane ($\varkappa_{xy}^T \neq 0$) distortion mode. All other BB stackings show a full population of the in-plane strain and curvature vectors, which is responsible for complex coupling and corresponding deformations. Table 6 summarized the cool-down induced strain and curvatures for the elements of 'twist-only' group, and Fig. 3 re-plots the corresponding warpage plots.

It can be seen in Table 6 that in-plane strains are in a comparable range for all eight 'twist-only' cases. Thus, in-plane CTEs of all laminates would be all very similar. Comparisons show, that mirroring

**Table 5**
Two-distinguishable population patterns, referring to Eq. (5).

| BB case | 'twist-only' $\lvert bb_1\rvert = \lvert bb_4\rvert$ and $\lvert bb_2\rvert = \lvert bb_3\rvert$ | All remaining |
|---|---|---|
| Population, Eq. (5) | $\begin{bmatrix}\neq 0\\ \neq 0\\ 0\\ 0\\ 0\\ \neq 0\end{bmatrix} = \begin{bmatrix}\bullet & \bullet & 0 & 0 & 0 & \bullet\\ \bullet & \bullet & 0 & 0 & 0 & \bullet\\ 0 & 0 & \bullet & \bullet & \bullet & 0\\ 0 & 0 & \bullet & \bullet & \bullet & 0\\ 0 & 0 & \bullet & \bullet & \bullet & 0\\ \bullet & \bullet & 0 & 0 & 0 & \bullet\end{bmatrix} \cdot \begin{bmatrix}\neq 0\\ \neq 0\\ 0\\ 0\\ 0\\ \neq 0\end{bmatrix}$ | $\begin{bmatrix}\neq 0\\ \neq 0\\ \neq 0\\ \neq 0\\ \neq 0\\ \neq 0\end{bmatrix} = \begin{bmatrix}\bullet & \bullet & \bullet & \bullet & \bullet & \bullet\\ \bullet & \bullet & \bullet & \bullet & \bullet & \bullet\\ \bullet & \bullet & \bullet & \bullet & \bullet & \bullet\\ \bullet & \bullet & \bullet & \bullet & \bullet & \bullet\\ \bullet & \bullet & \bullet & \bullet & \bullet & \bullet\\ \bullet & \bullet & \bullet & \bullet & \bullet & \bullet\end{bmatrix} \cdot \begin{bmatrix}\neq 0\\ \neq 0\\ 0\\ \neq 0\\ \neq 0\\ \neq 0\end{bmatrix}$ |

**Table 6**
Identified 'twist-only' cases.

| DD BB $r = 4$ for all | $\varepsilon_x^T$ $10^{-6}$/K | $\varepsilon_y^T$ $10^{-6}$/K | $\gamma_{xy}^T$ $10^{-6}$/K | $\varkappa_x^T$ $10^{-6}$/(m K) | $\varkappa_y^T$ $10^{-6}$/(m K) | $\varkappa_{xy}^T$ $10^{-6}$/(m K) |
|---|---|---|---|---|---|---|
| [15, 55, −55, −15] | 2.25 | 5.85 | **0.00** | **0.00** | **0.00** | 1.48 |
| [15, −55, 55, −15] | 2.15 | 5.82 | **0.00** | **0.00** | **0.00** | −0.16 |
| [−15, 55, −55, 15] | 2.15 | 5.82 | **0.00** | **0.00** | **0.00** | 0.16 |
| [−15, −55, 55, 15] | 2.25 | 5.85 | **0.00** | **0.00** | **0.00** | −1.48 |
| [55, 15, −15, −55] | 2.21 | 6.19 | **0.00** | **0.00** | **0.00** | 2.65 |
| [55, −15, 15, −55] | 2.11 | 6.16 | **0.00** | **0.00** | **0.00** | 2.21 |
| [−55, 15, −15, 55] | 2.11 | 6.16 | **0.00** | **0.00** | **0.00** | −2.21 |
| [−55, −15, 15, 55] | 2.21 | 6.19 | **0.00** | **0.00** | **0.00** | −2.65 |

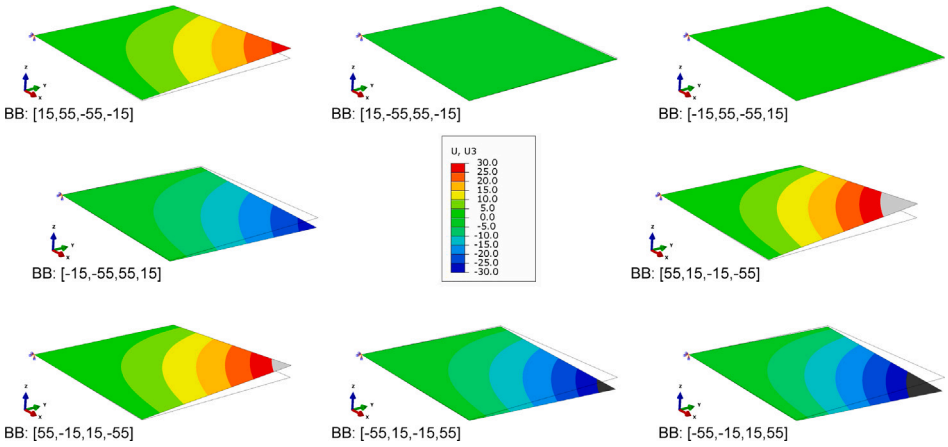


**Fig. 3.** Distortion of the identified 'twist-only' cases. Legend from Fig. 2.

a BB, as for example from $[15, 55, -55, -15]$ to $[-15, -55, 55, 15]$, does not affect in-plane strain magnitudes. However, the sign of the twist-curvature coefficient $\varkappa_{xy}$ changes, which is equivalent to changing the rotation of the twist deformation, as indicated above. In general, it can be concluded that the in-plane strain magnitudes are almost identical for all eight cases. In contrast, the twist coefficient $\varkappa_{xy}$ varies between $|0.16|$ and $|2.65|$, which corresponds to a remarkable scaling factor of 16.6. Table 7 summarizes the strain and curvature values for all 24 BB cases (with $r = 4$). Entries marked with $\star$ refer to the identified 'twist-only' group, with the $|bb_1| = |bb_4|$ and $|bb_2| = |bb_3|$ BB architecture. Cases, marked with •, are examined in an experimental validation spot check, presented in the following section.

- Only two selected BBs of the DD's total 24 building-block options show minimal distortions after cool down.
- The study reveals that inverting the building-block ply order leads to a sign change of the in-plane shear coefficient $\gamma_{xy}$ and the twist coefficient $\varkappa_{xy}$.
- The analysis reveals that curvature and twist is predominantly driven by in-plane thermal forces $N_x^T$ and $N_y^T$, leading to: $\left[\varkappa_x, \varkappa_y, \varkappa_{xy}\right]^T \approx [b] \cdot \left[N_x^T, N_y^T, N_{xy}^T\right]^T$
- A stacking sequence of type $[|\varphi|, |\psi|, |\psi|, |\varphi|]$ always result in $\gamma_{xy}^T = \varkappa_x^T = \varkappa_y^T = 0$ and $\varkappa_{xy}^T \neq 0$
- Depending on the stacking-sequence in the aforementioned building block, the twist-driving parameter $\varkappa_{xy}^T$ is found to scale between 0.16 and 2.65 (positive and negative). Thus, twist deformations are found up to 16.6 times higher for the worst BB selection in this group, compared to the best possible selection.
- For the study at hand, the BB blocks $[-15, 55, -55, 15]$ and $[15, -55, 55, -15]$. shows the lowest deformations due to cool down.
- Table 7 shows why the deformation character does not mirror for BB cases of the 'remaining' group. For those cases, one observes that only $\gamma_{xy}^T$ and $\varkappa_{xy}^T$ change sign, when the stacking is mirrored. As the in-plane strains $\varepsilon_x^T, \varepsilon_y^T$, and the out-of-plane curvatures $\varkappa_x^T, \varkappa_y^T$, do not change sign, both BB cases lead to individual superpositions.

### 3.2. Experimental spot check

Two 500 mm × 500 mm hardware samples were manufactured for a spot check of the presented numerical study. The selected configurations are: $[15, -55, 55, -15]_4$ denoted as 'mini' and $[-15, -55, 15, 55]_4$ denoted as 'maxi' hereafter. Both are marked with the symbol •, in Table 7. The samples were made from Hexcel M21E/IMA medium grade unidirectional prepreg (see ply data in Table 2). Optical measurements were executed to quantify warpage of both parts, after they have been

**Table 7**
Result summary of strain-curvature vector results.

| | DD BB $r = 4$ for all | $\varepsilon_x^T$ ppm/K | $\varepsilon_y^T$ ppm/K | $\gamma_{xy}^T$ ppm/K | $\varkappa_x^T$ ppm/(m K) | $\varkappa_y^T$ ppm/(m K) | $\varkappa_{xy}^T$ ppm/(m K) |
|---|---|---|---|---|---|---|---|
| | [15, −15, 55, −55] | 2.25 | 6.01 | −0.17 | 0.57 | −1.56 | 0.98 |
| | [15, −15, −55, 55] | 2.22 | 6.01 | 0.19 | 0.59 | −1.58 | −0.57 |
| | [15, 55, −15, −55] | 2.26 | 6.02 | −0.17 | 0.26 | −0.75 | 2.05 |
| ★ | [15, 55, −55, −15] | 2.25 | 5.85 | **0.00** | **0.00** | **0.00** | 1.48 |
| | [15, −55, −15, 55] | 2.12 | 5.99 | 0.19 | 0.30 | −0.78 | −1.17 |
| ★• | [15, −55, 55, −15] | 2.15 | 5.82 | **0.00** | **0.00** | **0.00** | −0.16 |
| | [−15, 15, 55, −55] | 2.22 | 6.01 | −0.19 | 0.59 | −1.58 | 0.57 |
| | [−15, 15, −55, 55] | 2.25 | 6.01 | 0.17 | 0.57 | −1.56 | −0.98 |
| | [−15, 55, 15, −55] | 2.12 | 5.99 | −0.19 | 0.30 | −0.78 | 1.17 |
| ★ | [−15, 55, −55, 15] | 2.15 | 5.82 | **0.00** | **0.00** | **0.00** | 0.16 |
| • | [−15, −55, 15, 55] | 2.26 | 6.02 | 0.17 | 0.26 | −0.75 | −2.05 |
| ★ | [−15, −55, 55, 15] | 2.25 | 5.85 | **0.00** | **0.00** | **0.00** | −1.48 |
| ★ | [55, 15, −15, −55] | 2.21 | 6.19 | **0.00** | **0.00** | **0.00** | 2.65 |
| | [55, 15, −55, −15] | 2.26 | 6.02 | 0.17 | −0.26 | 0.75 | 2.05 |
| ★ | [55, −15, 15, −55] | 2.11 | 6.16 | **0.00** | **0.00** | **0.00** | 2.21 |
| | [55, −15, −55, 15] | 2.12 | 5.99 | 0.19 | −0.30 | 0.78 | 1.17 |
| | [55, −55, 15, −15] | 2.25 | 6.01 | 0.17 | −0.57 | 1.56 | 0.98 |
| | [55, −55, −15, 15] | 2.22 | 6.01 | 0.19 | −0.59 | 1.58 | 0.57 |
| ★ | [−55, 15, −15, 55] | 2.11 | 6.16 | **0.00** | **0.00** | **0.00** | −2.21 |
| | [−55, 15, 55, −15] | 2.12 | 5.99 | −0.19 | −0.30 | 0.78 | −1.17 |
| ★ | [−55, −15, 15, 55] | 2.21 | 6.19 | **0.00** | **0.00** | **0.00** | −2.65 |
| | [−55, −15, 55, 15] | 2.26 | 6.02 | −0.17 | −0.26 | 0.75 | −2.05 |
| | [−55, 55, 15, −15] | 2.22 | 6.01 | −0.19 | −0.59 | 1.58 | −0.57 |
| | [−55, 55, −15, 15] | 2.25 | 6.01 | −0.17 | −0.57 | 1.56 | −0.98 |

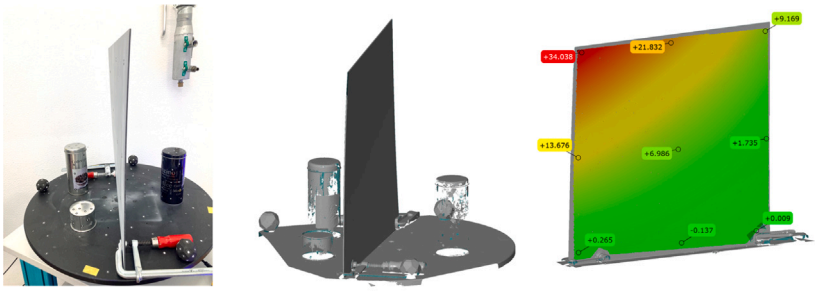


**Fig. 4.** Evaluation procedure using ZEISS ATOS system.

demolded and trimmed to final dimensions. Fig. 4 shows the executed evaluation procedure, which uses a rotary table combined with a ZEISS Atos scanner and the corresponding Inspect software for evaluation purposes.

The manufactured samples substantiate the general trend of the numerical study. A strong effect of the BB selection is found. The 'maxi' part shows considerable warpage, with almost 35 mm measured out-of-plane deformation. The 'mini' part shows little warpage, with the measurement showing an out of plane deformation of around 6 mm. Fig. 5 summarizes the spot-check, comparing the aforementioned distortions of the manufactured samples with the corresponding numerical predictions.

Overall, the experiments substantiate the numerical work. However, the observed discrepancy between the simulations and the measurements are found surprisingly high. The observed diverging trend is even more conspicuous, as larger deformation of the 'maxi' part is overestimated by the simulation, while the smaller deformation, of the 'mini' part, is underestimated.

More-detailed analysis has been executed, trying to explain the sources for the discrepancy. The respective section has been shifted to Appendix A.1 in the Appendix for sake of conciseness. The analyses focuses on

- the effect of the applied evaluation procedure,
- the effect of simulation-parameter uncertainty.

The analyses show that the selected boundary conditions for the FE model can be improved, as they cannot be directly mimicked when evaluating the measurement data. The effect of a more adequate selection is quantified in Fig. A.7.

A sensitivity study, on the effect of three main simulation parameters $E_1$, $\alpha_1$ and $\alpha_2$, reveals a very strong dependency of the simulated distortion results $u_3$ from these parameters. The study shows that many parameter combinations in the examined parameter ranges lead to an excellent match between measured and predicted deformation. The best eight combinations are summarized in Table A.9. The set $E_1 = 155$ GPa, $\alpha_1 = 0.4$ ppm/K, $\alpha_2 = 28$ ppm/K, for example, leads to a almost perfect match, with a $u_3$ discrepancy of 0.00061 mm only.

While both examined effects can explain some discrepancy, the observed diverging trend could not be explained entirely. Nonetheless, the spot check underlines the importance of an adequate BB selection, when minimum warpage is desired. However, the experiments, also show that even the 'best' identified BB selection 'mini' leads to multiple mm warpage on part level, when a 3 mm DD laminate is made from only four building blocks.

### 3.3. A brief comment on extrapolation of findings

Typical questions in DD context are: 'What happens when the number of repeats is changed, while the laminate thickness remains constant, which refers to a potential thin-ply application or 'What

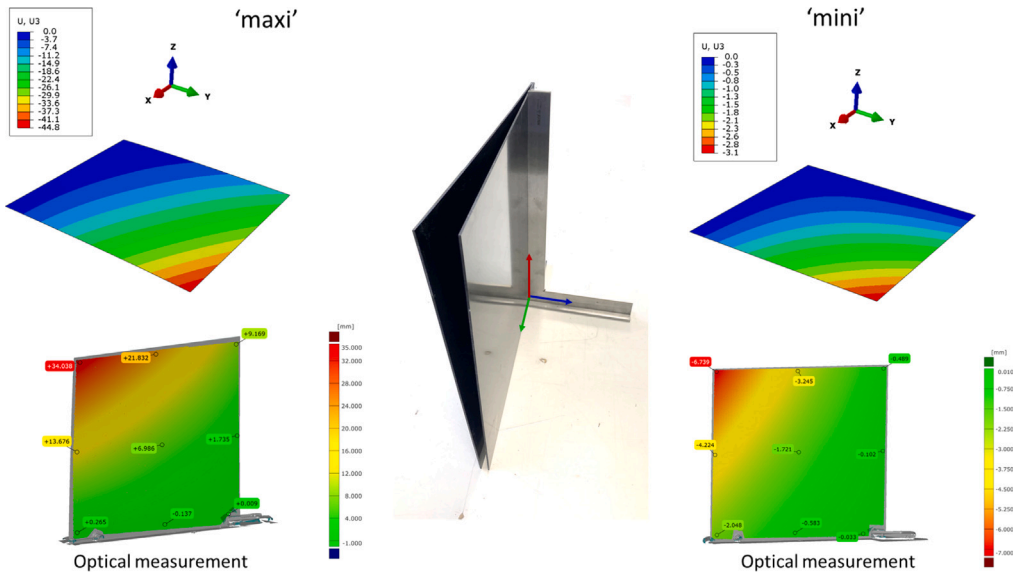


**Fig. 5.** Experimental spot check - numerical results, measured deformation of manufactured parts.

**Table 8**
Result summary - generic cases.

| DD for all | $\epsilon_x^T$ ppm/K | $\epsilon_y^T$ ppm/K | $\gamma_{xy}^T = \varkappa_x^T = \varkappa_y^T$ | $\varkappa_{xy}^T$ ppm/(m K) |
|---|---|---|---|---|
| $[15, 55, -55, -15]_{4, t_{ply}=0.184\ mm}$ | 2.25 | 5.85 | 0.00 | **1.48** |
| $[15, 55, -55, -15]_{8, t_{ply}=0.184\ mm}$ | 2.18 | 5.82 | 0.00 | **0.36** |
| $[15, 55, -55, -15]_{16, t_{ply}=0.184\ mm}$ | 2.16 | 5.82 | 0.00 | **0.09** |
| $[15, 55, -55, -15]_{8, t_{ply}=0.092\ mm}$ | 2.18 | 5.82 | 0.00 | **0.72** |
| $[15, 55, -55, -15]_{16, t_{ply}=0.046\ mm}$ | 2.16 | 5.82 | 0.00 | **0.36** |

happens when the number of repeats and the laminate thickness is changed?

This section provides a brief analysis on those simple questions. The previous simulation results and the manufactured parts refer to the specific laminate with 16 plies (r = 4) and 2.944 mm nominal laminate thickness. Hereafter the following five generic scenarios are examined:

1. Reference: $(r = 4)$, $t_{ply} = 0.184$ mm, $t_{lam} = 2.944$ mm
2. Doubled repeats, doubled laminate thickness
3. Quadrupled repeats, quadrupled laminate thickness
4. Doubled repeats, halved ply thickness (=Reference laminate thickness) (see detailed results in Appendix A.2)
5. Quadrupled repeats, quartered ply thickness (=Reference laminate thickness)

The latter two cases assume that corresponding generic ply thicknesses are available for the prepreg at hand. This is linked to thin-ply developments, but rather generic for most prepreg types, which are on the marked right now. Table 8 summarizes the results for the five cases, in the same format of the tables above. The examples refer to the BB $[15, 55, -55, -15]$, which belongs to the $|bb_1| = |bb_4|$, $|bb_2| = |bb_3|$ group.

The previous table suggests the following conclusions:

- When the number of repeats of the reference is multiplied by a factor $k$, and the thickness increase is considered, on observes a scaling of the curvature coefficients with $1/k^2$.
- When the number of repeats of the reference is multiplied by a factor $k$, while constant laminate thickness is preserved, due to the use of thinner plies, one observes a scaling of the curvature coefficients with $1/k$. Fig. 6 shows that this scaling effects transfers directly to the warpage distortions (case 'mini' shown).
- It is found that the particular deformation characteristic does neither change when the ply thickness nor the number of BB repeats change. One only observes scaling for the curvature coefficients. The strain coefficient remain almost identical.

## 4. Conclusion and outlook

The present study focuses on the family of Double–Double (DD) laminates, which are composed of a repeated stack of 4-ply building blocks (BBs), while each BB is composed of the plies $+\varphi, -\varphi, +\psi, -\psi$. An example 16-ply laminate can be written $[+\varphi, -\psi, -\varphi, +\psi]_4$. It represents a stack of four BBs, without additional symmetry constraints.

Manufactured samples of the authors indicate that the stacking sequence, within the BB, is decisive whether a flat laminate shows almost no or considerable warpage. 24 conceivable BB stacking sequences exist, which makes it difficult for designers to pick the 'best' one.

The present study examined the relation between the BB's stacking-sequence and corresponding part warpage. The study consists of FE-analysis, analytical analysis to explain observations and an experimental spot check to verify the findings. Due to research-project boundaries, the study focuses on the ply orientation ±15° and ±55°. However, major findings can be extrapolated to other similar laminates, as independent results of a parallel study from Hawkins et al. indicate.

The main conclusions from the current work are as follows:

1. The study shows, that a DD laminate will always show twist, as the coefficient $\varkappa_{xy} \neq 0$ is found for all BB cases. However, the effective warpage magnitude in mm depends and scales with the number of BB repeats.
2. The analytical work shows that all conceivable 24 stacking sequences can be separated in the two groups 'twist-only' and 'remaining'.
3. The 'twist-only' group has eight members.
   It consists of all BBs with $[\pm\varphi, \mp\psi, \pm\psi, \mp\varphi]$ stacking.
4. Inverting the BB stacking sequence, for one of the 'twist-only' laminates, inverts the deformation pattern.

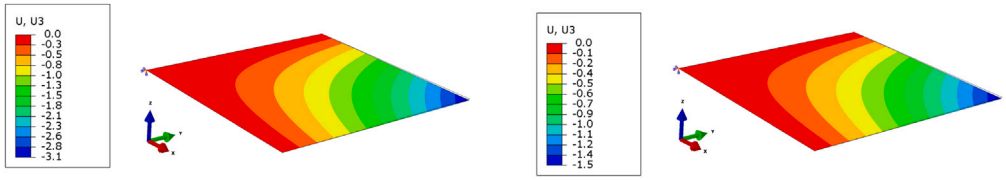


(a) Case 1: $[15, -55, 55, -15]_4$, $t_{ply} = 0.184$ mm (b) Case 4: $[15, -55, 55, -15]_8$, $t_{ply} = 0.092$ mm

**Fig. 6.** Effect of doubling the number of repeats at constant laminate thickness for 'Mini' stacking (Case 4 in enumeration above)

5. Laminate of the 'remaining' group show a fully populated strain-curvature vector. Thus, those laminates show a complex superposition of in-plane and out-of-plane distortion modes, when subjected to a temperature change.
6. A dedicated study on the effect of BB repeat shows that the process of homogenization transfers to warpage of flat laminates. It is shown that doubling the number of repeats and therefore the laminate thickness scales the twist coefficient $\varkappa_{xy}$ by a factor of 1/4. When the repeats are doubled, while the ply-thickness is halved the twist coefficient $\varkappa_{xy}$ scales by a factor of 1/2. At the same time, the in-plane strain-properties (in-plane CTEs) do not change more than 5%.
7. The BB stackings $[\pm 15, \mp 55, \pm 55, \mp 15]$, both members of the 'twist-only' group, shows the smallest distortions within the simulation, with a minimum $\varkappa_{xy} = \mp 0.16$. This finding is in line with a parallel published study of Hawkins et al. [16] who presented a 'minimum-warpage' DD laminate with a [+9/−61.5/+61.5/−9] BB.

## CRediT authorship contribution statement

**Erik Kappel:** Writing – original draft, Visualization, Validation, Methodology, Investigation, Formal analysis, Data curation. **Ronald Klomp:** Writing – review & editing, Conceptualization.

## Disclaimer

Funded by the European Union. Views and opinions expressed are however those of the authors only and do not necessarily reflect those of the European Union or Clean Aviation Joint Undertaking. Neither the European Union nor the granting authority can be held responsible for them.

## Declaration of competing interest

The authors declare that they have no known competing financial interests or personal relationships that could have appeared to influence the work reported in this paper.

## Acknowledgment

The project '101101974 - UP Wing' is supported by the Clean Aviation Joint Undertaking and its members.


## Appendix

### *A.1. Discrepancy assessment in the experimental spot check effect of the applied evaluation procedure*

The applied boundary conditions in the simulation model are idealized, as only a single node is clamped. In fact, displacements $(u_x, u_y, u_z)$ and rotations $(ur_x, ur_y, ur_z)$ of the single corner node are constrained in the models. The evaluated $u_3$ displacements refer to the $z$-axis, and the scalar values represent node distances to the xy-plane (normal to z) in the deformed state. The evaluation of the measurement data pursues a slightly deviating strategy. Perfectly mimicking the idealized BCs of the FE model is impossible. The sample parts are clamped with a screw clamp in one corner, in order to hold them in fixed position, during the measurement on a rotary table. The evaluation plane for quantifying warpage is defined based on the measurement data. The plane is defined by three manually selected points on the measured surface, as Fig. A.7(a) shows. This approach is accompanied by the risk that the defined plane does not perfectly represent a tangential plane, as it is the case in the idealized FE model. Even slight tilting of the pink plane in Fig. A.7(a) affects the distance evaluation to that plane. Already a little deviation of 1°, for example, induces a discrepancy of around 8–9 mm for the 500 mm long sample. Fig. A.7(b) shows the effect in the FE model, when four nodes, close to the corner, are used for the corresponding boundary condition.

The boundary condition adaptation directly affects the $u_3$ displacement magnitude, as shown in Fig. A.7(b). The updated boundary conditions are used within the following parameter sensitivity study, as it is considered more realistic. It is examined, whether the measured displacement of the 'maxi' case (−34 mm in Fig. 5) can be reached when the specific simulation parameters are modified. Therefore, the maximum displacement in the FE model is evaluated, while the difference to the measurement is evaluated as $|\Delta u| = |u_3^{sim} - (-34)\ \text{mm}|$.

*Simulation parameter uncertainty*

Table 2 provides the parameter set, used for the analyses of the present paper. Even though the CTE data has been determined in an earlier study using TMA measurements there remains some uncertainty. The Young's modulus values usually differ for tension and compression. Thus, the 154 GPa value from the literature is likely an average value. A parametric study has been conducted to assess the sensitivity of the deformation analysis. The examined parameter ranges are: $E_1$ in range [144, 164, steps: 1] GPa, $\alpha_1$ in range [0, 2, steps: 0.2] ppm/K and $\alpha_2$ [28, 32, steps: 1] ppm/K. Thus, 1155 calculations were examined in total $(21 \cdot 11 \cdot 5)$.

Table A.9 provides the eight parameter combination, which show the smallest deviation between measurement and simulation.

This excerpt clearly underlines the high sensitivity of the performed simulation. Multiple excellent result are found, with completely different parameter configurations.

**Table A.9**
Top-eight parameter combination, with minimum discrepancy between simulation and measurement for the maxi case.

| $E_1$ GPa | $\alpha_1$ ppm/K | $\alpha_2$ ppm/K | $\|\Delta\|$ mm | $E_1$ GPa | $\alpha_1$ ppm/K | $\alpha_2$ ppm/K | $\|\Delta\|$ mm |
|---|---|---|---|---|---|---|---|
| 155 | 0.4 | 28 | 0.00061 | 163 | 1.4 | 30 | 0.00851 |
| 147 | 1.4 | 28 | 0.00138 | 158 | 2.0 | 30 | 0.02152 |
| 163 | 0.4 | 29 | 0.00349 | 150 | 2.0 | 29 | 0.02626 |
| 155 | 1.4 | 29 | 0.00433 | 158 | 1.0 | 29 | 0.02646 |

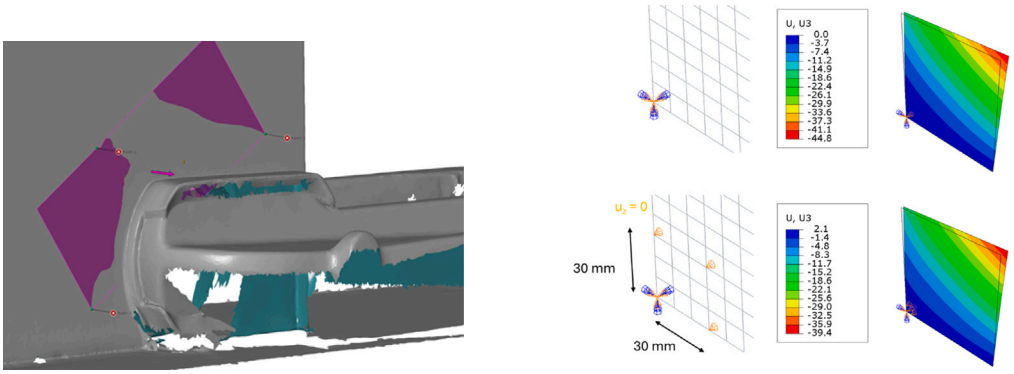


(a) Ref. plane definition in measurement data. Red points define the evaluation reference

(b) Effect of updated ref. plane definition on $u_3$ displacements

**Fig. A.7.** Effect of an alternative evaluation strategy on the $u_3$ deformation.

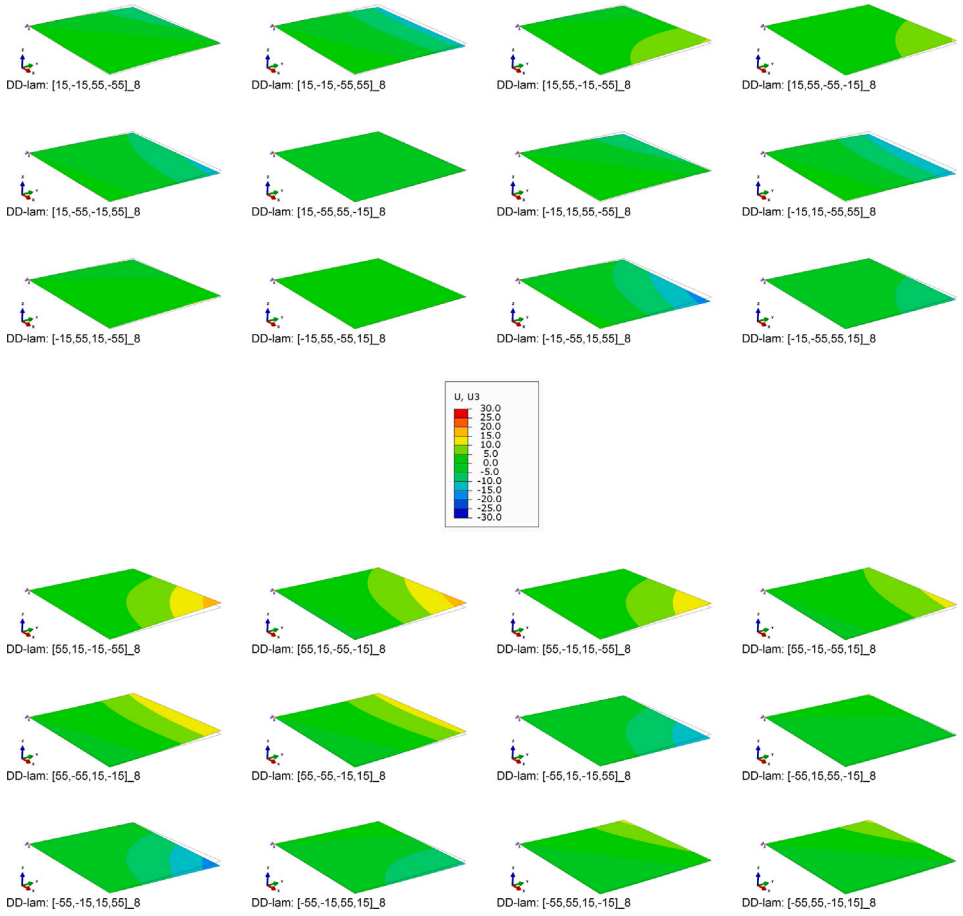


**Fig. A.8.** Distortion of all 24 conceivable building-block configuration $[\pm 15°/\pm 55°]_8$, for $t_{ply} = 0.092$ mm.

### *A.2. Generic case example: doubled repeats, halved ply thickness*

The effect of BB repeats $r$ is often discussed. Hereafter, a particular scenario is examined which is focused on $r$. The study examines laminates with doubled repeats (8 instead of 4). The ply-thickness is halved to assure the same total laminate thickness. The image collection in Fig. A.8 shows the corresponding warpage plots. They can directly be compared with the plots shown in Fig. 2.

One can observe the $1/r$-scaling when strains and curvatures in Table A.10 are compared with the initial results provided in Table 7.

### *A.3. Reference ABAQUS *.inp file*

Parametric input file for ABAQUS analysis. Note, that bb1, bb2, bb3 and bb4 are inserted as ply angles. Node locations, element definitions and the final composite laminate definition needs to be added, according to the shown patterns.

## Data availability

No data was used for the research described in the article.

Listing 1: Parametric *.inp files skeleton

```
*Heading
*Preprint, echo=NO, model=NO, history=NO, contact=NO
*Part, name=Part-1
*Node
      1,           0.,           0.,           0.
      2,          10.,           0.,           0.
 ...
   2600,         490.,         500.,           0.
   2601,         500.,         500.,           0.
*Element, type=S4R
   1,    1,    2,   53,   52
   2,    2,    3,   54,   53
...
2500, 2549, 2550, 2601, 2600
*Elset, elset=_Surf-1_SPOS, internal, generate
    1,  2500,     1
*Surface, type=ELEMENT, name=Surf-1
_Surf-1_SPOS, SPOS
*Distribution, name=Ori-1-DiscOrient, location=ELEMENT, Table=Ori-1-DiscOrient_Table
,           1.,           0.,           0.,           0.,           1.,           0.
1,           1.,          -0.,           0.,           0.,           1.,          -0.
2,           1.,          -0.,           0.,           0.,           1.,          -0.
....
2499,           1.,          -0.,           0.,           0.,           1.,          -0.
2500,           1.,          -0.,           0.,           0.,           1.,          -0.
*Orientation, name=Ori-1, system=RECTANGULAR
Ori-1-DiscOrient
3, 0.
*Elset, elset=CompositeLayup-1-1, generate
    1,  2500,     1
** Section: CompositeLayup-1-1
*Shell Section, elset=CompositeLayup-1-1, composite, orientation=Ori-1, layup=CompositeLayup-1
0.184, 3, M21E,bb1, Ply-1
0.184, 3, M21E,bb2, Ply-2
...
0.184, 3, M21E,bb3, Ply-15
0.184, 3, M21E,bb4, Ply-16
*End Part
*Instance, name=Part-1-1, part=Part-1
*End Instance
*Nset, nset=BCZ, instance=Part-1-1
 1,
*Nset, nset=ALL_nodes, instance=Part-1-1, generate
    1,  2601,     1
*End Assembly
*Distribution Table, name=Ori-1-DiscOrient_Table
coord3D, coord3D
*Material, name=M21E
*Elastic, type=LAMINA
154000.,8500., 0.32,4200.,4200.,2500.
*Expansion, type=ORTHO
 1.5e-06, 3.22e-05,       0.
*Initial Conditions, type=TEMPERATURE
ALL_nodes, 160.
*Step, name=Step-1, nlgeom=YES
*Static
1., 1., 1e-05, 1.
*Boundary
BCZ, 1, 1
BCZ, 2, 2
BCZ, 3, 3
BCZ, 4, 4
BCZ, 5, 5
BCZ, 6, 6
*Temperature
ALL_nodes, 0.
*Restart, write, frequency=0
*Output, field, variable=PRESELECT
*Output, history, variable=PRESELECT
*End Step
```

**Table A.10**
Result summary - generic case.

| | DD BB $r = 8$ for all | $\varepsilon_x^T$ ppm/K | $\varepsilon_y^T$ ppm/K | $\gamma_{xy}^T$ ppm/K | $\varkappa_x^T$ ppm/(m K) | $\varkappa_y^T$ ppm/(m K) | $\varkappa_{xy}^T$ ppm/(m K) |
|---|---|---|---|---|---|---|---|
| | [15, −15, 55, −55] | 2.18 | 5.86 | −0.04 | 0.28 | −0.77 | 0.50 |
| | [15, −15, −55, 55] | 2.17 | 5.86 | 0.05 | 0.28 | −0.77 | −0.29 |
| | [15, 55, −15, −55] | 2.18 | 5.86 | −0.04 | 0.14 | −0.38 | 1.00 |
| ★ | [15, 55, −55, −15] | 2.18 | 5.82 | 0.00 | 0.00 | 0.00 | 0.72 |
| | [15, −55, −15, 55] | 2.15 | 5.86 | 0.05 | 0.14 | −0.38 | −0.57 |
| ★ | [15, −55, 55, −15] | 2.16 | 5.82 | 0.00 | 0.00 | 0.00 | −0.08 |
| | [−15, 15, 55, −55] | 2.17 | 5.86 | −0.05 | 0.28 | −0.77 | 0.29 |
| | [−15, 15, −55, 55] | 2.18 | 5.86 | 0.04 | 0.28 | −0.77 | −0.50 |
| | [−15, 55, 15, −55] | 2.15 | 5.86 | −0.05 | 0.14 | −0.38 | 0.57 |
| ★ | [−15, 55, −55, 15] | 2.16 | 5.82 | −0.00 | 0.00 | 0.00 | 0.08 |
| | [−15, −55, 15, 55] | 2.18 | 5.86 | 0.04 | 0.14 | −0.38 | −1.00 |
| ★ | [−15, −55, 55, 15] | 2.18 | 5.82 | −0.00 | 0.00 | 0.00 | −0.72 |
| ★ | [55, 15, −15, −55] | 2.17 | 5.90 | 0.00 | 0.00 | 0.00 | 1.29 |
| | [55, 15, −55, −15] | 2.18 | 5.86 | 0.04 | −0.14 | 0.38 | 1.00 |
| ★ | [55, −15, 15, −55] | 2.15 | 5.90 | 0.00 | 0.00 | 0.00 | 1.08 |
| | [55, −15, −55, 15] | 2.15 | 5.86 | 0.05 | −0.14 | 0.38 | 0.57 |
| | [55, −55, 15, −15] | 2.18 | 5.86 | 0.04 | −0.28 | 0.77 | 0.50 |

(*continued on next page*)

**Table A.10** (*continued*).

| | DD BB $r = 8$ for all | $\varepsilon_x^T$ ppm/K | $\varepsilon_y^T$ ppm/K | $\gamma_{xy}^T$ ppm/K | $\varkappa_x^T$ ppm/(m K) | $\varkappa_y^T$ ppm/(m K) | $\varkappa_{xy}^T$ ppm/(m K) |
|---|---|---|---|---|---|---|---|
| | [55, −55, −15, 15] | 2.17 | 5.86 | 0.05 | −0.28 | 0.77 | 0.29 |
| ⋆ | [−55, 15, −15, 55] | 2.15 | 5.90 | −0.00 | 0.00 | 0.00 | −1.08 |
| | [−55, 15, 55, −15] | 2.15 | 5.86 | −0.05 | −0.14 | 0.38 | −0.57 |
| ⋆ | [−55, −15, 15, 55] | 2.17 | 5.90 | −0.00 | 0.00 | 0.00 | −1.29 |
| | [−55, −15, 55, 15] | 2.18 | 5.86 | −0.04 | −0.14 | 0.38 | −1.00 |
| | [−55, 55, 15, −15] | 2.17 | 5.86 | −0.05 | −0.28 | 0.77 | −0.29 |
| | [−55, 55, −15, 15] | 2.18 | 5.86 | −0.04 | −0.28 | 0.77 | −0.50 |

## References


[1] S.W. Tsai, Double-Double: New family of composite laminates, AIAA J. (2021) http://dx.doi.org/10.2514/1.J060659.

[2] S.W. Tsai, et al., DOUBLE-DOUBLE a New Perspective in the Manufacture and Design of Composites, JEC/ Stanford publication, ISBN: 978-0-9819143-3-6, 2022.

[3] E. Kappel, Y. Boose, M. Missbach, A CAI study on transition zones of conventional and Double-Double laminates, Compos. Part C: Open Access 14 (2024) 100450.

[4] E. Kappel, Double-Double laminates for aerospace applications - finding best laminates for given load sets, Compos. Part C: Open Access 8 (2022) 100244.

[5] E. Kappel, Buckling of simply-supported rectangular Double-Double laminates, Compos.: Part C (Open Access) (2023).

[6] E. Kappel, S.W. Tsai, Double-Double laminates - A review on the status quo in spring 2024, 2024, http://dx.doi.org/10.57965/g2cb-8t21, Open Source at: https://elib.dlr.de/204753/.

[7] A. Vescovini, C.X. Li, J.P. Mendez, B.C. Jin, A. Manes, C. Bisagni, Post-buckling behavior and collapse of Double-Double composite single stringer specimens, Compos. Struct. 327 (2024) 117699.

[8] D. Zerbst, L. Tönjes, S. Dähne, E. Werthen, E. Kappel, C. Hühne, Equivalent plate formulation of Double-Double laminates for the gradient-based design optimization of composite structures, Compos. Struct. 354 (2025) 118786.

[9] D.W. Radford, Shape Stability in Composites (Ph.D. thesis), Rensselaer Polytechnic Institute, 1987.

[10] G. Fernlund, A. Poursartip, Getting part dimensions right in composites molding, Compos. World Mag. (2015).

[11] A.A. Johnston, An Integrated Model of the Development of Process-Induced Deformation in Autoclave Processing of Composite Structures (Ph.D. thesis), The University of New Brunswick, 1992.

[12] E. Kappel, Process Distortions in Composite Manufacturing - from an Experimental Characterization To a Prediction Approach for the Global Scale (Dissertation), Otto-von-Guericke-University Magdeburg, Germany, 2013.

[13] E. Kappel, D. Stefaniak, C. Hühne, Process distortions in prepreg manufacturing - An experimental study on CFRP L-profiles, Compos. Struct. 106 (2013) 615–625.

[14] D. Stefaniak, D. Kappel, T. Spröwitz, C. Hühne, Experimental identification of parameters inducing warpage of autoclave-processed CFRP parts, Compos.: Part A 43 (2012) 1081–1091.

[15] E. Kappel, Forced-interaction and spring-in - Relevant initiators of process-induced distortions in composite manufacturing, Compos. Struct. 140 (2016) 217–229.

[16] A. Hawkins, S.L.J. Millen, A. Aravand, Homogenisation of Double-Double (DD) laminates: Warpage mitigation and new stacking sequence approaches, J. Compos. Mater. (2025).

[17] A.T. Nettles, Basic Mechanics of Laminated Composite Plates - NASA Reference Publication 1351, Technical Report, NASA, 1994.

[18] R. Talreja, J. Varna, Modeling Damage, Fatigue and Failure of Composite Materials, Woodhead Publishing, Elsevier, 2016.

[19] E. Kappel, R. Prussak, On abnormal thermal-expansion properties of more orthotropic M21E/IMA carbon-fiber-epoxy laminates, Compos. Commun. 17 (2020) 129–133.